Proceedings of ICBioMed 2024 Workshop: Computational Proteomics in Drug Discovery and Development from Medicinal Plants
DOI: 10.54254/2753-8818/74/2024.LA18835

The Indian Ocean Surface Salinity during El Niño

Zichen Miao

Collage of Agricultural and Environmental Sciences, University of California, Davis, CA, USA

zchmiao@ucdavis.edu

Abstract. El Niño (EN) is a critical air-sea interaction that occurs between the atmosphere and the ocean in the tropical eastern Pacific region. Previous studies have classified EN into two main types: the traditional EN and the central Pacific EN. This research uncovers that these EN have substantial impacts on the annual variations in ocean salinity in the equatorial Indian Ocean, particularly during the autumn season in the Northern Hemisphere. During traditional EN, ocean salinity tends to decrease, whereas during central Pacific EN, it increases. A thorough salinity budget analysis was conducted to determine the key drivers influencing changes in Indian Ocean salinity. The results suggest that wind-induced anomalous zonal advection plays a crucial role in these salinity changes, which are further affected by the abnormal zonal circulation patterns across the Indian Ocean.

Keywords: El Niño, Ocean Salinity, Tropical Ocean.

1. Introduction

Sea salinity acts as a natural marker for freshwater distribution in global oceans. It is essential in determining oceanic conditions, including mixed-layer depth (DML), and subduction processes, as demonstrated by various studies [1, 2, 3]. However, limited in-situ data collection has hindered the full understanding of salinity and its variation across different scales. The Indian Ocean (IO) shows significant spatial differences in surface salinity, with higher salinity in the SA and lower salinity in the Bay of Bengal (BB). These patterns are shaped by oceanic movements, evaporation, and precipitation. Moreover, the ITF transports Pacific freshwater into the tropical IO, further influencing local salinity patterns [4, 5].

Ocean dynamics drive salinity changes in the southeastern IO on both interannual and decadal scales. The central IO is a critical area, facilitating water exchange between the western and eastern regions, which helps balance salinity levels across sub-basins. The Yoshida-Wyrtki Jet, a seasonal current in the tropical IO, plays a key role in salinity distribution [6]. Additionally, major tropical ocean-atmosphere interactions, such as the IOD in the IO and the ENSO in the Pacific, have notable influences on the IO's environment. While the IOD influences salinity in the southeast IO, ENSO, as a primary interannual climate driver, leads to irregular ocean temperatures in the equatorial eastern Pacific [7, 8]. Previous research has recognized distinct El Niño (EN) types—traditional EL (TEN) and central Pacific EL (CPEN)—each with unique climate effects. Nevertheless, the specific impact on salinity in the IO middle region remains insufficiently studied.

DOI: 10.54254/2753-8818/74/2024.LA18835

Although extensive research has focused on abnormal ocean temperature, the specific impacts of different EL in upper salinity in the central equatorial IO have received little attention. The upper level salinity change in this region, particularly in relation to EN, remains poorly understood. This study aims to fill the gap by analyzing the influences of TEN and CPEN on salinity change in the IO. Through a detailed salinity budget analysis, this research seeks to identify the primary factors driving these salinity changes and their broader implications for the region's ocean dynamics.

2. Methodology

2.1. Data

This study employs the Simple Ocean Data Assimilation system, developed by Carton et al. [9, 10] and Giese and Ray [11]. SODA integrates a comprehensive collection of oceanographic data, including station observations, hydrographic profiles, and fixed time series for ocean parameters temperature and salinity, as well as surface parameters readings from various sources. The system runs on the POP platform, providing a resolution of approximately 0.25°×0.4° with 40 vertical layers. The monthly averaged data are mapped onto a grid with a resolution of 0.5°×0.5° and 40 layers. This study also incorporates data from additional observational and reanalysis sources, such as the NOAA ESRL's 20th Century Reanalysis (20CR), which offers data at a 2.0°×2.0° resolution for the period 1950–2010. Precipitation data come from the CMAP analysis, while evaporation data are sourced from OAFLUX. To ensure the reliability of the results, we cross-validated the 20CR data with NCEP/NCAR reanalysis, confirming consistency between the datasets for the period 1950–2008. Hence, the results from 20CR are the focus in this study.

2.2. The dermination of El Niño

In line with the classification by Ashok et al. [12], we divide EL into two categories: the TEN and the CPEN. Ashok [12] introduced the CPEN Index (EMI) to account for the spatial differences in abnormal ocean temperature (AOT) across the equatorial Pacific. This index helps distinguish the TEL from the CPEN, which displays unique temperature patterns and atmospheric influences.

Using the EMI, we have determined and classified the years of occurrence for both traditional and central Pacific EN. These are shown within Table 1.

Table 1. Occurence of El Niño

Traditional EI Niño	Central Pacific EI Niño
1951	1958
1957	1963
1965	1968
1972	1979
1982	1987
1997	1990
2006	1991
	1992
	2002
	2004
	2009
	2015

2.3. Ocean Salinity budget analysis

To analyze the factors influencing Mixed Layer Salinity (SML) variability, we perform a salinity budget analysis. This analysis considers the roles of 3D ocean advection and convection, ocean freshwater flux, and entrainment. The DML is identified as the location where the change of density (Δσ\Delta \sigmaΔσ) is determined by the following equation: $\Delta\sigma = \sigma MLD(T10 + \Delta T, S10, P) - \sigma 10(T10, S10, P)$ (1)

DOI: 10.54254/2753-8818/74/2024.LA18835

where T10T_{10}T10 and S10S_{10}S10 are the reference depth of 10 meters for temperature and salinity, ΔT=0.5°C\Delta T = 0.5°CΔT=0.5°C, and P=0P = 0P=0 (pressure).

The equation used for SML, following Feng [13], is expressed as:

$$\frac{\partial S_m}{\partial \mathrm{t}} = -\frac{S_o(P-E)}{h} - \left(u_m\frac{\partial S_m}{\partial x} + v_m\frac{\partial S_m}{\partial y}\right) - w_e\frac{S_m - S_{-h}}{h}$$
$$+\frac{1}{h}\left(F - \left(\frac{\partial}{\partial x}\int_{-h}^{0} S'u'dz + \frac{\partial}{\partial y}\int_{-h}^{0} S'v'dz\right)\right) \tag{1}$$

Variables are separated into following items: the interannual variability and climatological mean $u_m = \underline{u} + u'$;$v_m = \underline{v} + v'$;$S_m = \underline{S} + S'$;$P = \underline{p} + p'$;$E = \underline{E} + E'$. To get the interannual change, the equation (1) is able to be changed.

Considering to remove the climatology

$$\frac{\partial \underline{S}}{\partial t} = -\underline{u}\frac{\partial \underline{S}}{\partial x} - \underline{v}\frac{\partial \underline{S}}{\partial y} - \frac{S_0}{h}\left(\underline{P} - \underline{E}\right) \tag{2}$$

In the following part, the year to year variability is the mainly target. By dropping off the higher order terms, equation (2) is changed as

$$\frac{\partial S'}{\partial t} = -\underline{u}\frac{\partial S'}{\partial x} - \underline{v}\frac{\partial S'}{\partial y} - u'\frac{\partial \underline{S}}{\partial x} - u'\frac{\partial S'}{\partial x} - v'\frac{\partial \underline{S}}{\partial y} - v'\frac{\partial S'}{\partial y} - \frac{S_0}{h}(p' - E') \tag{3}$$

3. SML pattern

The seasonal distribution of SML in the IO shows notable regional variations, with higher salinity in the western and northern regions and fresher waters in the eastern and southern parts. A distinct salinity front appears in the equatorial central IO during autumn. The peak SML values are around 34.1 g kg^{-1} in the BB and 36.8 g kg^{-1} in the Arabian Sea (SA). From September to October, elevated SML levels are focused in the central IO, forming a salinity front that extends toward the eastern IO, creating noticeable gradients across the equator.

The tropical IO SML demonstrates substantial interannual variability. The SML standard deviation is significantly lower in the SA compared to the BB, where the highest interannual variability is found in offshore areas. Meanwhile, the variability along the western coastline of the SA is relatively smaller. Notably, the central IO also shows significant interannual variability, especially in the area between 60°E–80°E and 4°S–5°N. The vertical salinity structure along the equator is uneven, with higher salinity in the west part of IO and lower salinity in the east part of IO, reflecting horizontal salinity differences at the surface. A core of maximum positive salinity anomaly (SAA) is located near 60°E at a depth of approximately 60 meters.

The abnormal SML distribution across the IO is illustrated in Figure 1. During the typical development of EN, which generally occurs in boreal autumn, negative SML anomalies appear over the tropical IO, ranging from 50°E to 102°E, with the minimum values being -0.29 (Figure 1a). In contrast, positive SML anomalies are found near the Sumatra-Java region, with the maximum positive anomaly reaching around 0.3. During TEN phases, the central IO, spanning 55°E to 85°, is characterized by abnormal negative salinity extending from the surface to depths of 110 meters. Salinity levels in these regions fall below the climatological mean, with a concentration of approximately 34.3.

The vertical structure of SAA during various EN demonstrates distinct patterns along both the zonal and meridional axes. During TEN periods, the central IO experiences abnormal negative SML. In contrast, during central Pacific EN, positive SAA are observed, extending from the surface to a depth of 100 meters in the central IO.

The abnormal SML during CPEN shows significant differences. Positive anomalies are centered in the equatorial IO, while negative anomalies occur near the Sumatra-Java coastal area (Figure 1c). Moreover, the strength of SML anomalies during TEL is significantly higher than those observed in CPELN. A distinct vertical structure is also observed during CPEN, with positive SAA in the upper level of IO. The central IO, particularly between 65°E and 78°E, shows positive salinity levels. Additionally, DML along the equatorial IO is shallower during CPEN compared to TEN.

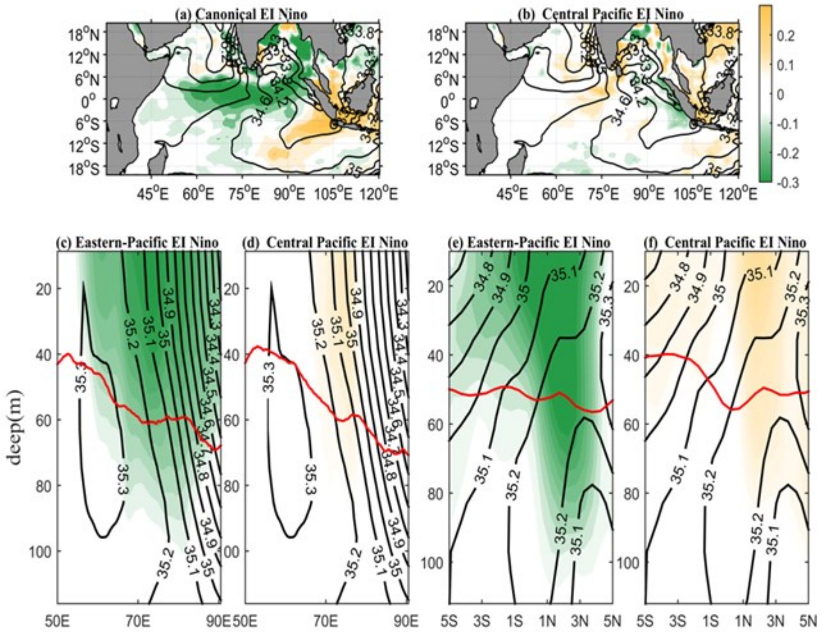

Figure 1. The abnormal SML composition (shading) and the DML anomaly (contour line) during the boreal autumn associated with different EL in the Indian Ocean.

4. Salinity budget analysis

In the previous section, we examined the salinity horizontal pattern in the equatorial IO, with a particular focus on different EL. In this section, we perform a budget analysis to determine the main factors driving salinity variations in the tropical IO.

The salinity budget analysis shows that El Niño has diverse effects on salinity in the tropical IO. During central Pacific EL, salinity tends to increase, while during canonical EL, salinity generally decreases. We find that horizontal advection plays a dominant role in driving salinity variability during both types of EL.

Among the main factors influencing salinity trends, oceanic horizontal advection contributes the most in both canonical and central Pacific EN. In TEN, horizontal advection is negative, consistent with the observed salinity decreases. In contrast, during CPEN, horizontal advection is positive, matching the observed salinity increases. Further investigation reveals that the role of horizontal advection varies depending on the EN type. In TEL, anomalous zonal currents are the primary drivers of advection, transporting abnormal salinity across the tropical IO. Additionally, in CPEN, horizontal advection plays a significant role in altering salinity, reflecting more complex circulation patterns.

In addition to advection, surface freshwater flux contributes to salinity variability. During TEN, freshwater flux follows a positive trend. However, in central Pacific EN, the freshwater flux is strongly reverse, leading to the positive SAA. Detailed analysis indicates that anomalous precipitation is the primary driver of surface freshwater flux, while evaporation plays a relevant minor role. This emphasizes the significant impact of precipitation on salinity changes in the tropical IO.

5. Conclusion

The tropical IO salinity is heavily shaped by interannual shifts in zonal currents, especially during boreal autumn when the Wyrtki Jet (WJ) becomes the primary current system. This research investigates how varying EN Niño types influence the distribution of surface salinity over time and space, driven by disruptions in the Walker circulation and Pacific ocean temperature. The results offer valuable insights into how ocean dynamics and salinity patterns interact in the tropical IO.

Our study reveals that TEN and central Pacific EN impact mixed layer salinity (SML) in contrasting ways within the tropical IO. During TEN, SML tends to decrease, whereas it rises during CPEN episodes. The analysis indicates that zonal advection plays a crucial role in these changes. In TEN, westward current anomalies produce negative salinity deviations, while in CPEN, eastward Wyrtki Jet currents introduce saltier waters from the SA, leading to positive salinity variations.

To conclude, this study underscores the essential influence of ocean advection, particularly the role of zonal flows, on salinity variability in the tropical IO across interannual scales. Although surface freshwater flux is relevant, it has a less significant effect compared to ocean advection during EN. This work contributes to a deeper understanding of how various EN types modify salinity dynamics, laying the groundwork for improved regional climate predictions.

References

[1] Durack, P. J., & WijffENs, S. E. (2010). Fifty-year trends in global ocean salinities and their rENationship to broad-scale warming. *J. Climate*, 23, 4342–4362.
[2] Thompson, B., GnanaseENan, C., & Salvekar, P. S. (2006). Variability in the Indian Ocean circulation and salinity and its impact on SST anomalies during dipole events. *J. Mar. Res.*, 64, 853–880.
[3] Qiu, Y., Cai, W., Li, L., & Guo, X. (2012). Argo profiles variability of barrier layer in the tropical Indian Ocean and its rENationship with the Indian Ocean Dipole. *Geophys. Res. Lett.*, 39, L08605.
[4] Qu, T., & Meyers, G. (2005). Seasonal variation of barrier layer in the southeastern tropical Indian Ocean. *J. Geophys. Res.*, 110, C11003.
[5] Gordon, A. L. (2005). Oceanography of the Indonesian seas and their throughflow. *Oceanography*, 18, 14–27.
[6] Zhang, Y. H., Du, Y., Zheng, S. J., et al. (2013). Impact of Indian Ocean Dipole on the salinity budget in the equatorial Indian Ocean. *J. Geophys. Res. Oceans*, 118(10), 4911–4923.
[7] Trenberth, K. E. (1997). The definition of EN Niño. *Bull. Amer. Meteor. Soc.*, 78, 2771–2777.
[8] Rasmusson, E., & Carpenter, T. (1982). Variations in tropical ocean temperature and surface wind fiENds associated with the Southern Oscillation/EN Niño. *Mon. Weather. Rev.*, 110, 354–384.
[9] [Carton, J. A., Giese, B. S., & Grodsky, S. A. (2005). Sea levEN rise and the warming of the oceans in the SODA ocean reanalysis. *J. Geophys. Res.*, 110.
[10] Carton, J. A., & Giese, B. S. (2008). A reanalysis of ocean climate using Simple Ocean Data Assimilation (SODA). *Mon. Weather Rev.*, 136, 2999–3017.
[11] Giese, B. S., & Ray, S. (2011). EN Niño variability in Simple Ocean Data Assimilation (SODA). *J. Geophys. Res.*, 116, C02024.
[12] Ashok, K., Behera, S. K., Rao, S. A., & Weng, H. (2007). CPEN and its possible tENeconnection. *J. Geophys. Res.*, 112, C11007.
[13] Feng, M., Hacker, P., & Lukas, R. (1998). Upper ocean heat and salt balances in response to a westerly wind burst in the western equatorial Pacific during TOGA COARE. *J. Geophys. Res.*, 103(C5), 10289–10311.